Magnetoelastic coupling, negative thermal expansion, and two-dimensional magnetic excitations in FeAs

J. L. Niedziela,[1,*,†] L. D. Sanjeewa,[2,*] A. A. Podlesnyak,[3] L. DeBeer-Schmitt,[3] S. J. Kuhn,[2] C. de la Cruz,[3] D. S. Parker,[2] K. Page,[3,4] and A. S. Sefat[2]

[1]*National Security Sciences Directorate, Oak Ridge National Laboratory, Oak Ridge, Tennessee 37831, USA*
[2]*Materials Science & Technology Division, Oak Ridge National Laboratory, Oak Ridge, Tennessee 37831, USA*
[3]*Neutron Scattering Division, Oak Ridge National Laboratory, Oak Ridge, Tennessee 37831, USA*
[4]*Materials Science and Engineering Department, University of Tennessee, Knoxville, Tennessee 37996, USA*

(Received 26 May 2020; revised 28 January 2021; accepted 26 February 2021; published 19 March 2021)

We present a temperature-dependent investigation of the local structure and magnetic dynamics of the FeAs binary. The magnetic susceptibility $\chi(T)$ result shows an anomalous broad feature up to 550 K, with χ continuing to increase above the Néel antiferromagnetic ordering temperature ($T_N = 70$ K), peaking at ~250 K, then decreasing gently above. It is remarkable that this peak susceptibility temperature corresponds to the onset of anisotropic negative thermal expansion in both the *a* and *c* axes, suggesting that magnetic interactions are affecting the structure even well above the Néel point. A systematic investigation into local bonding correlations, from time-of-flight neutron pair distribution function analyses, shows the octahedral volume around each Fe site growing monotonically while adjacent octahedra tilt toward one another before relaxing away past this peak in the anomalous magnetic susceptibility. We use inelastic-neutron scattering to map spin-wave excitations in FeAs at temperatures above and below the T_N. We find magnetic excitations near T_N to be very different from the excitations in the ground state at 1.5 K. Spin waves measured at 1.5 K are three dimensional (3D), however, in the vicinity of the magnetic transition, the magnetic fluctuations clearly indicate two-dimensional (2D) character in this intrinsically 3D crystal structure. Unlike the undoped 2D parents of iron-arsenide superconductors, where the magnetic correlations are considerably weaker along the *c* axis than in the *ab* plane, inelastic neutron scattering here shows that the spin fluctuations in the 3D FeAs binary are nearly 2D in the *bc* plane at 90 K. These results demonstrate the importance of short-range correlations in understanding the magnetic properties of transition-metal binaries, and suggest how 2D excitations, even in a 3D structure, can potentially become a breeding ground for unconventional superconductivity.

DOI: 10.1103/PhysRevB.103.094431

I. INTRODUCTION

The iron-arsenide binary, FeAs, can be a template structure for potential iron-arsenide superconductors. While structurally distinct from the iron-arsenide superconductors, FeAs is reported to have an interplay of incommensurate spin-density wave (SDW) and itineracy [1], favoring the highly anisotropic transport and magnetization properties characteristic of the iron-arsenide superconductors [2]. The discovery of ferropnictide [3] and chalcogenide [4] superconductors has generated interest in exploring interactions between crystal and magnetic structure, short range correlations, magnetic dynamics, and unconventional superconductivity [5,6]. Understanding the nature of Fe-As bonds and Fe-Fe interactions of this simple iron-arsenide binary may therefore help to answer fundamental questions underlying the difference between FeAs-binary and iron-arsenide superconductors, which enable both magnetic and Cooper pair interactions.

The FeAs structure is shown in Fig. 1. The reported structure is orthorhombic, *Pnma* (MnP type), with two unique Fe sites. Earlier attempts to establish the structure of FeAs vacillated on the structure as *Pnma* or $Pna2_1$, where each Fe would possess slightly different arsenic coordination [7]. Due to the relatively small differences between the two models [7,8], the slightly higher symmetry *Pnma* is traditionally used. No structural transition is reported in the literature prior to the melting point near 1325 K [8]. Figure 1(a) shows the unit cell with two (out of the total four) distorted $FeAs_6$ octahedral units depicted. In the *Pnma* configuration, the Fe sits at the 4*c* Wyckoff position, which results in each site possessing an equivalent set of long, short, and intermediate Fe-As distances. The labels assigned to each atom are derived from our lower symmetry labeling used in the modeling. In this construct, each Fe site has two sets of equal length bonds in the buckled equatorial position, and two significantly longer axial bonds of distinct length which are each slightly distorted away from the central symmetry axis of the octahedron [7]. The face sharing $FeAs_6$ octahedra are connected in an alternating network linked through the long axial (L_a) and short axial (S_a) bond distances, respectively, as shown in Fig. 1(b). Additionally, these $FeAs_6$ octahedra interconnect with each other along the *b* and *c* axes via sharing edges.

FeAs is reported to have a noncollinear SDW structure below $T_N = 70$ K, with incommensurate ordering at 4 K

*These authors contributed equally to this work.
†Corresponding author: niedzielajl@ornl.gov

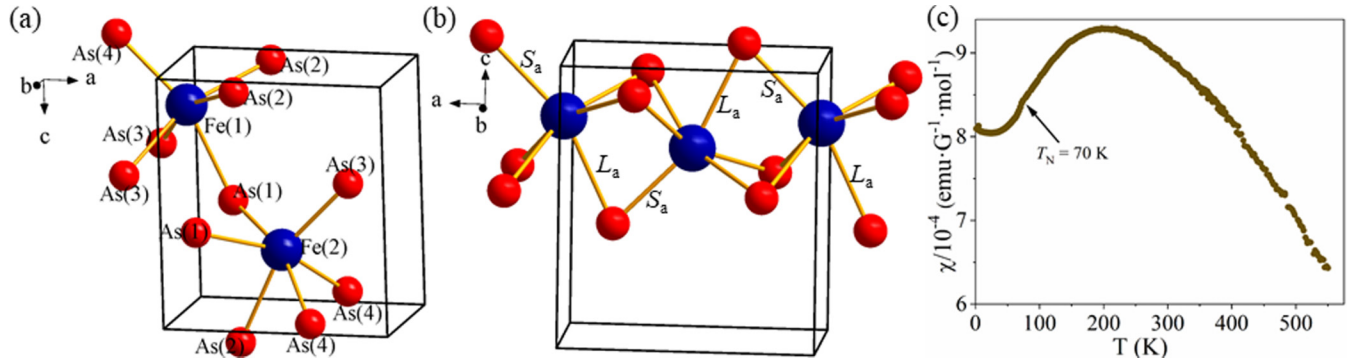

FIG. 1. Two views of the FeAs structure: (a) The distorted $FeAs_6$ octahedra, where Fe ions are sixfold coordinated by As. Bonds belonging to the buckled equatorial plane of each octahedra are of equal length, while the axial bonds are separated into long axial (L_a) and short axial (S_a) bond distances. (b) The bonding network between the octahedra, where the bonding connections alternate between short and long axial connections along the *a* axis. (c) Magnetic susceptibility of FeAs, showing T_N at 70 K with a broad anomalous hump centered around 250 K.

[1]. In the nonmagnetic phase, Mössbauer experiments show lattice-magnetic interactions and anisotropic local susceptibility of Fe above T_N [9], for which we find additional evidence here. The magnetic susceptibility exhibits broad regions at high temperatures that may suggest some type of short-range ordering [2], while significant deviations in resistivity are noted between the *b* and *c* axes [2,10]. In a similar manner to the iron-arsenide superconductors, computational reports on FeAs fail to fully capture the correct static structure and magnetic properties [11,12], suggesting a role for the subtle local structural effects that we study here.

Moreover, the superconductivity in iron arsenides manifests with doping from metallic parent compounds unlike the cuprates, which exhibit superconductivity near a correlated Mott insulating state. As was pointed out by Paglione and Greene [6], although the origin of Cooper pairing in two-dimensional (2D) iron arsenides remains unidentified, a large amount of circumstantial evidence points to magnetic spin fluctuations. Therefore, much work has been done to study spin dynamics in the parent compounds, for example those of AFe_2As_2 (A = Ba, Sr, Ca) [13–17], NaFeAs [16,18], and $FeTe_{1-x}Se_x$ [19] (see also a review by Lumsden and Christianson [5]). The observed overall energy scales are about 200–260 meV, suggesting strong effective magnetic exchange couplings in iron arsenides similar to the exchange couplings hallmark to cuprates. Spin waves in iron-arsenide superconductors are well defined at low energies, however much broader at energies above 100 meV, suggesting that itinerant electrons play an important role. There is no consensus among researchers whether the observed magnetic excitations can be described with a simple Heisenberg Hamiltonian [14,17], itinerant scenarios [13,15], or a model that combines both local moment and itinerant electrons [20,21]. To this end, the spin dynamics in the simplest iron arsenide, the binary FeAs, are of fundamental importance for understanding the interplay between magnetism and 2D spin excitations which could lead to unconventional superconductivity in these materials.

Also, important here are deviations from long-range crystal symmetry observed from local atomic configuration studies, which have been shown to be critical in understanding the behaviors of the iron-arsenide superconductors [22,23]. Understanding the coupling of the structure to magnetism, and the role of the local environment of Fe in the structure, may provide clues to the rich physics in the future development in this type of research. This is of particular relevance to understanding the suppression of static magnetism and nematic fluctuations. To investigate short-range structural correlations in FeAs, we performed neutron pair distribution function (PDF) analyses, and find that the variation in octahedral volume around the iron site tracks closely with the anomalous susceptibility data. Additionally, by using inelastic neutron scattering (INS) we find evidence that in the vicinity of T_N, 2D-like spin fluctuations prevail in this 3D crystal structure. Moreover, we find the weakest structural exchanges to be along the *a* axis, suggesting *bc*-layered structure motifs at room temperature, contrary to iron-arsenide superconductors that are comprised of *ab* layers separated in the *c* direction.

II. EXPERIMENTAL DETAILS

A. Synthesis

FeAs materials were produced following Saparov *et al.* [24]. The FeAs binary phase was synthesized using Fe powder (Alfa Aesar 99.99%) and As pieces (Alfa Aesar 99.99%). In a typical reaction, Fe and As were mixed in 1:1 stoichiometry and loaded into a silica ampoule before sealing under vacuum. As the first step, the reaction mixture was heated to 700 °C (20 °C/h, dwell 12 h). Then, the temperature was raised to 1065 °C (dwell 24 h) before furnace-cooling to room temperature. After the reaction, the resulting grey metallic powder was ground inside the glove box. Further details on the growth method of FeAs single crystals are described in Ref. [6]. 1.2 g of sample were prepared for the INS experiments, and the purity of the sample was confirmed using powder x-ray diffraction.

B. Neutron diffraction

Time of flight neutron powder diffraction data were collected at the Nanoscale Ordered Materials Diffractometer (NOMAD) instrument at the Spallation Neutron Source (SNS) at Oak Ridge National Laboratory (ORNL) [25]. Powdered samples were loaded and sealed into vanadium cans, and data were collected from 2 to 500 K using a liquid-helium

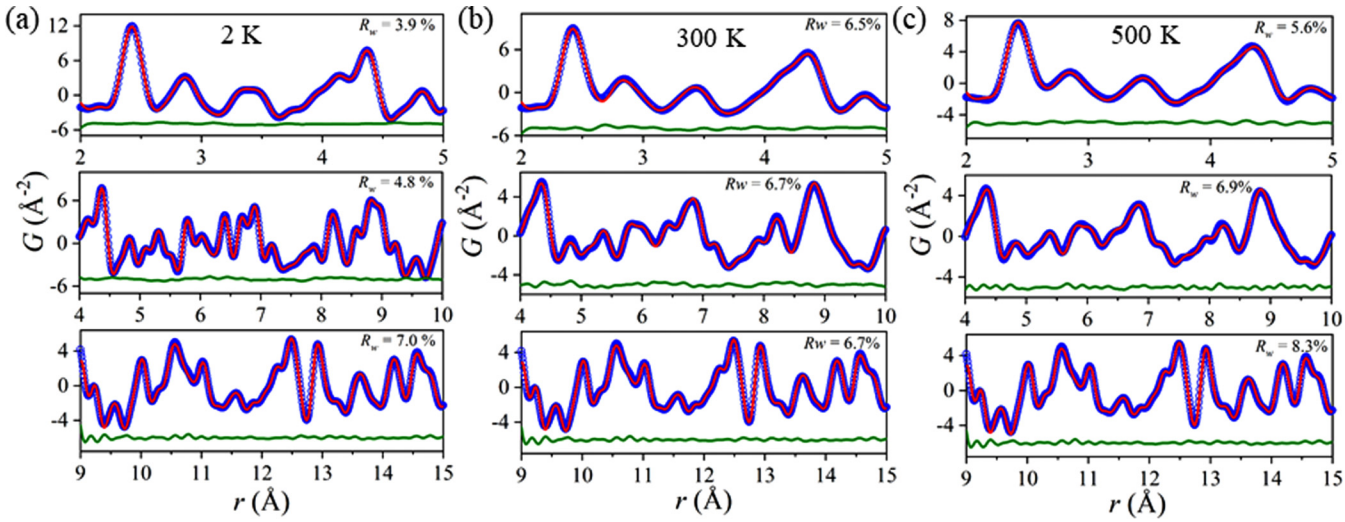

FIG. 2. Representative PDF data and *P1* model fits for 2-, 300-, and 500-K data as a function of fitting range r. Experimental data are shown as blue circles, modeled PDF as red lines, and green lines the model-data residual. R_w values reflect the model goodness of fit.

cryostat from 2 to 300 K, and a high-temperature displex for studies above 300 K up to 500 K. Standard calibrations were perfomed for all instrument setups. Data were reduced using interactive data language routines, and structural modeling and refinement of structural models against the PDF data was performed using PDFGUI [26].

C. Inelastic neutron scattering

Inelastic neutron scattering measurements were done using the Cold Neutron Chopper Spectrometer (CNCS) [27,28] and the Fine Resolution Chopper Spectrometer (SEQUOIA) [29] at SNS. Data were collected using fixed incident neutron energies of 81.8 meV for SEQUOIA, and 10.0 meV (3.1 meV) for CNCS, which allowed for the measurement of excitations up to energy transfers of $\hbar\omega$ 65 meV (SEQUOIA) and 8 meV (CNCS). In these configurations, a full width at half maximum (FWHM) resolution of 4.1 meV (SEQUOIA) and 0.06 meV (CNCS) was obtained at the elastic position. The FeAs crystal was mounted in the *H0L* scattering plane. Measurements were conducted on SEQUOIA at temperatures ranging from 5 to 90 K, while on CNCS measurements are performed from1.5 to 90 K. The excitation spectra were recorded by making full 360° rotations with a 1° step. The MANTIDPLOT [30] and DAVE [31] software packages were used for data reduction and analysis.

III. RESULTS AND DISCUSSION

Modeling of PDF data employed the starting structure of *Pnma*, which was found to be a reasonable overall match to the data, with some discrepancies at the local (low real space range) correlations. Congruence of the model and data were improved by forcing the *P1* symmetry condition and using r dependent fitting ranges. Representative data from 2, 300, and 500 K are shown in Fig. 2. Model refinements included the lattice parameters, Fe and As positions within the unit cell, and the isotropic atomic displacement parameters. The three r ranges employed include a region from 2 to 5 Å which corresponds to the short-range correlations and atomic environments of the individual octahedra, 4–10 Å, which represents the interoctahedral environment, and 9–15 Å for longer range correlations between octahedral units.

Temperature dependent lattice parameters and bond distances extracted from the short-range fitting results are shown in Fig. 3. The lattice parameter measurements as a function of temperature are consistent with literature studies, with the c and a axes contracting until 300 K, and the b axis showing continuous growth, Fig. 3(a) [2,24]. Fe-As distances depicted in Fig. 3(b) are extracted from the short-range fitting data describing the intraoctahedral coordination. The axial Fe-As bonds describe the distance of the apical As to the central Fe of the octahedra, with alternating orientation of short and long axial bonds above the equatorial plane for adjacent octahedra. The temperature dependent evolution of the Fe-As axial bonds show continual increase as a function of temperature, with a sharp rise between 200 and 300 K. Correspondingly, there is a steady increase in the length of the equatorial bonds in the distorted central plane of the octahedra. Taken together, these increasing bond distances demonstrate a steady increase in the octahedral volume surrounding the Fe ion, which reaches a maximum distortion at ∼250 K, corresponding to the peak in anomalous magnetization shown in Fig. 1(c). Similar information about the relative orientation of the octahedra is obtained from the As-As distances derived from the short-range PDF models, Fig. 3(c). The value of the distance between As(2) and As(3) (Fig. 1) corresponds to the distance from apical As of one octahedral unit to the equatorial As of the neighboring unit, demonstrating a relative tilt of the octahedral units as the temperature is raised. The Fe-Fe distances (not shown here) also indicate that the Fe-Fe distance between octahedral units along the c axis are most highly dependent on temperature, compensating for the increasing canting of the relative Fe-As octahedral units. Fitting results from the higher-r range modeling depicted in Fig. 2 indicate similar, though somewhat less pronounced, temperature dependent structural trends. These highlight the local nature of the structural distortions.

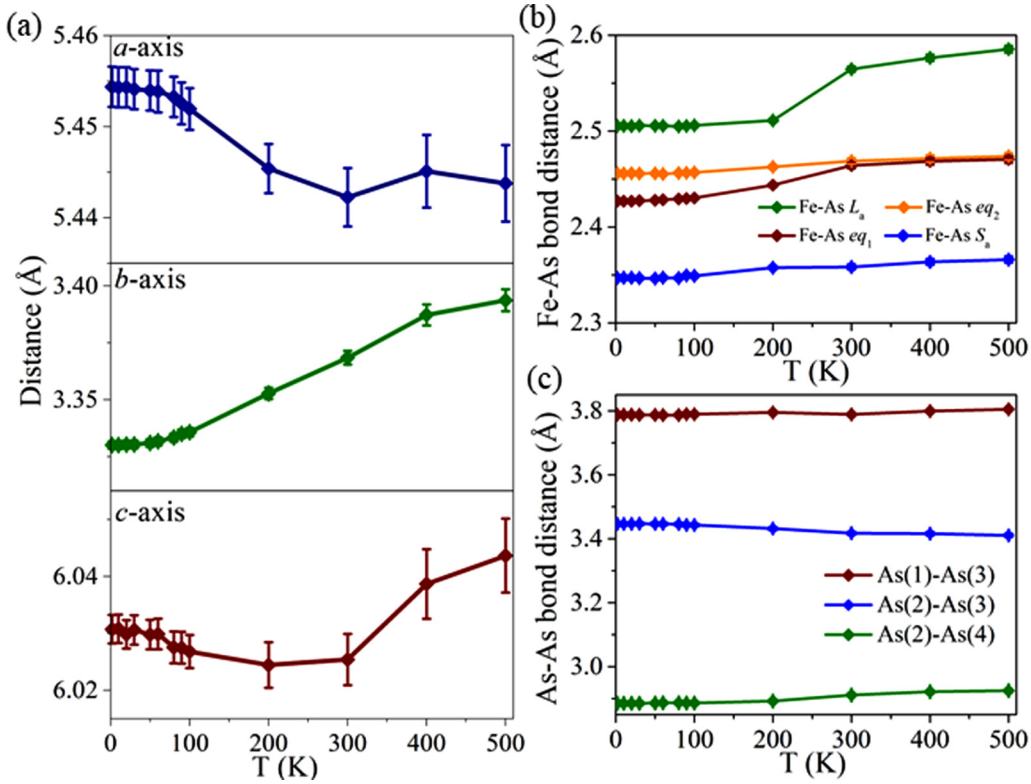

FIG. 3. (a) Change of unit cell parameters with temperature. (b) Temperature dependence of Fe-As short axial (S_a), long axial (L_a), and equatorial (eq_1, eq_2) bonds. (c) Temperature dependence of As-As bond distances (using the labeling in Fig. 1). All the parameters were derived from the PDF models resulting from 2- to 5-Å range fits to data.

Closely related to these structural features is the highly anisotropic thermal expansion, including negative thermal expansion (NTE) between 0 and 300 K in both the *a* and *c* axes and a substantial *positive* thermal expansion—some 1.2%—along the *b* axis. In particular, it is notable that the onset temperature of the NTE, between 250 and 300 K, is very close to the temperature of the susceptibility maximum—not the Néel temperature. Previous work on the spinel $LiGaCr_4S_8$ [32] finds an NTE whose onset temperature of approximately 100 K matches the deviation of the susceptibility from $1/T$ behavior, although in that cubic material the NTE is of course isotropic. Here in this relatively complex 3D structure there is an equally complex NTE behavior.

In our first principles calculations, as in previous work by one of us, the Fe-Fe exchange interactions in the calculated ground state are antiferromagnetic for Fe-Fe neighbors roughly along the *a* and *c* axes, but ferromagnetic along the *b* axis. In fact, despite this relatively large third nearest-neighbor Fe-Fe distance (3.375 Å at 300 K), it was found not possible to stabilize a state with antiferromagnetic interactions along the *b* axis, which suggests some degree of itinerant character here, despite the finding of a substantial local moment in the calculations. Here we have used the plane-wave density functional theory code WIEN2K [33], within the generalized gradient approximation of Perdew, Burke, and Ernzerhof [34].

We also note that the thermal expansion along the *b* axis is rather large—a 1.2% increase, relative to $T = 1.5$ K at 300 K. Indeed, previous data [35] find a 6.5% increase in this axis at 1300 K, while the corresponding 1300-K increase for the *a* axis is less than 0.5%. Clearly the complex 3D structure is driving these differences in thermal expansion, which is further affected by the appearance of magnetism at low temperature.

It is noteworthy that the NTE only occurs for the directions in which antiferromagnetic interactions are dominant, while the normal and substantial positive thermal expansion occurs in the direction of ferromagnetic interactions. When one combines this with the previous observation [11] that the distance dependence of exchange interactions does not follow the usual monotonic decrease with distance, along with the tantalizing correspondence of the susceptibility maximum temperature with the onset of NTE, one is left with a strong sense that all these unusual facts are somehow related, and that the NTE ultimately originates from the onset of magnetism and the detailed interaction of the magnetic energetics with the more common energies such as the phonon free energy.

Returning to the magnetic order itself, the neutron diffraction scattering map on the single crystal sample at $T = 1.5$ K confirms incommensurate magnetic order, Figs. 4(a) and 4(b). At low temperature, Figs. 4(c) and 5(a), the spin excitation spectrum is 3D and gapped, with an incommensurate modulation vector $q \sim 0.4c^*$, consistent with results from the literature [1]. Above T_N, Figs. 4(d) and 5(b), the spin excitations go from gapped to gapless, reflecting a transition to a two-dimensional state exhibiting short range magnetic order. Our data suggest that the spin-wave bandwidth of FeAs,

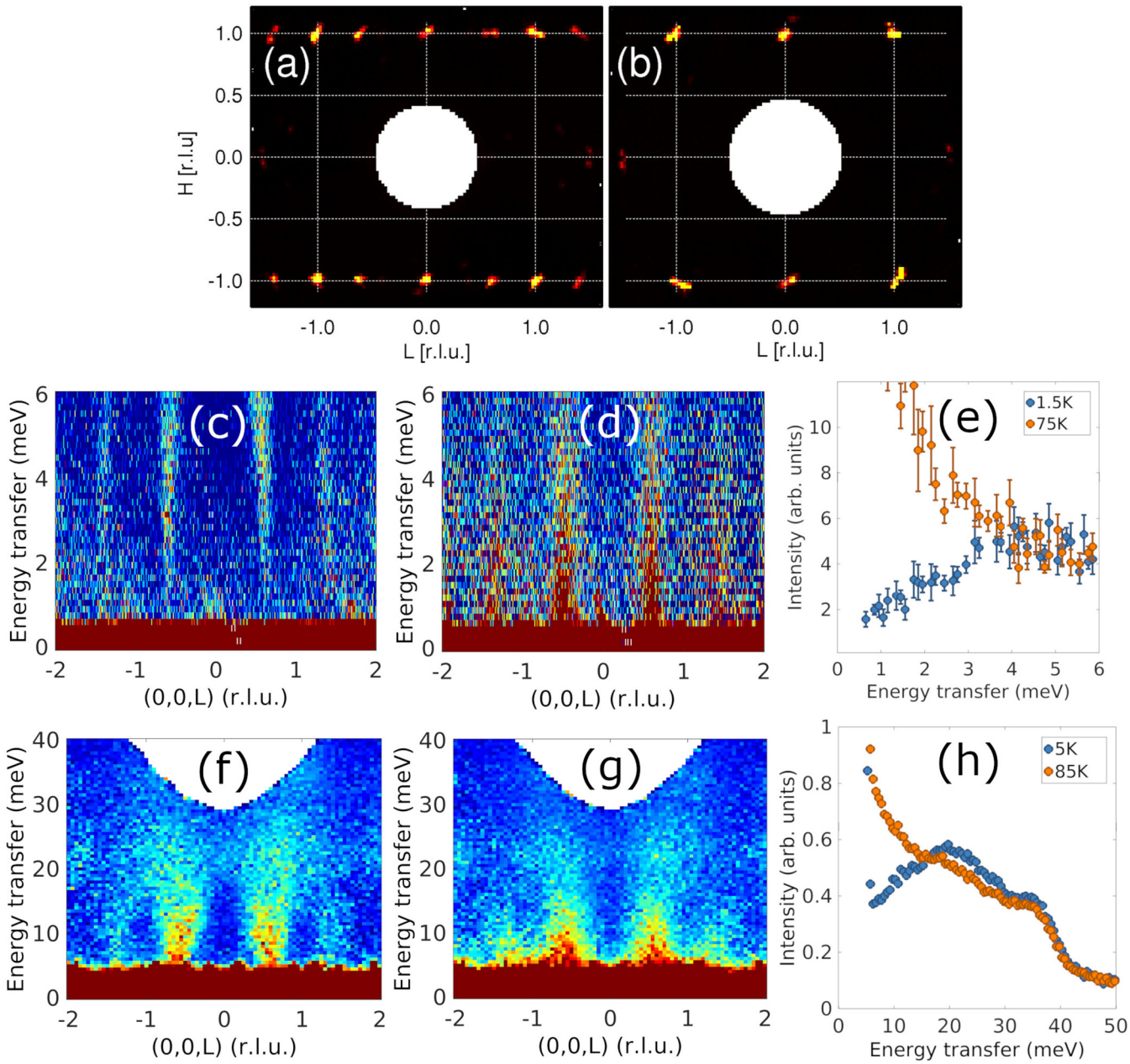

FIG. 4. Elastic neutron scattering map of FeAs at temperature (a) $T = 1.5$ K and (b) $T = 75$ K in the ($H0L$) scattering plane. (c) Low-energy part of magnetic excitations along the (10L) direction taken at CNCS at $T = 1.5$ K, (d) $T = 75$ K. The intensity is averaged over an interval of ± 0.05 reciprocal lattice units (r.l.u.) in the H and K directions. (e) The energy cuts at the antiferromagnetic wave vector at $T = 75$ K, indicating the opening of the spin-wave energy gap at low temperature. (f) The INS spectra taken at SEQUOIA in the (10L) direction at $T = 5.0$ K, and (g) $T = 85$ K, i.e., in the antiferromagnetic and paramagnetic state. The intensity is averaged over an interval of ± 0.1 r.l.u. in the H and K directions. (h) Energy dependence of the inelastic signal integrated within one Brillouin zone for $T = 5$ and 85 K, demonstrating that the spin-wave bandwidth of FeAs is ~ 35 meV. For better energy coverage and statistics we symmetrized the data according to the crystal symmetry before integration.

$\sim$35 meV, is considerably reduced from that of iron-arsenide superconductors which is around 200–250 meV [35]. It is known that in iron pnictides antiferromagnetic fluctuations remain into the paramagnetic phase region above T_N, where long-range order is already absent [5,32,36]. What comes as a surprise is an apparent shape of the magnetic excitations. As one can see in the constant energy slice, the magnetic excitations become anisotropic at $T = 90$ K (Fig. 5). The magnon intensity extends in the H direction and forms stripes, reflecting a collapse of coherence along a^*, while remaining coherent along c^*. Unlike the undoped 2D parents of iron-arsenide superconductors, where the magnetic correlations are considerably weaker along the c axis than in the ab plane, inelastic neutron scattering here shows that the spin fluctuations

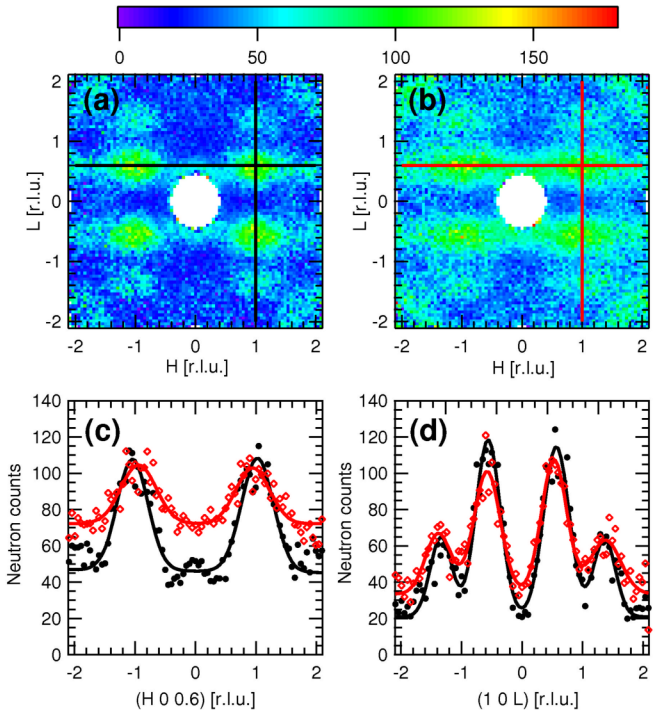

FIG. 5. Constant energy transfer $\hbar\omega = 12$ meV slices in the ($H0L$) plane taken at SEQUOIA at temperatures (a) $T = 5.0$ K, and (b) $T = 90$ K. Inelastic features at the corners around $\mathbf{q} = (\pm 2\ 0\ \pm 2)$ are phonons. (c), (d) Q dependence of the spin wave excitations below (filled black circles) and above (open red diamonds) T_N obtained through constant energy cut as shown by solid lines in the upper panels. Lines are guide to the eyes for the observed scattering.

in the 3D FeAs binary are nearly 2D in the bc plane at 90 K. This observation is further supported by the nature of $FeAs_6$ connectivity in the FeAs structure where $FeAs_6$ share edges along the bc plane and share faces along the a axis. The edge sharing nature of the $FeAs_6$ octahedra could facilitate a pseudo-2D Fe-Fe lattice in the 3D FeAs structure.

Thus, we find that the steady change observed in octahedral volume and relative octahedral tilting as a function of temperature via PDF track closely the anomalous magnetization measurements, with the maximal adjustment to the octahedral volume occurring near the maximal value for magnetization. The apical As within the $FeAs_6$ octahedra diverging to generate two distinct bond distances, and the equatorial As ions continually expanding, is reflective of a continuous Jahn-Teller type distortion. The subsequent octahedral tilt reflects the retained coherence along the c^* direction up to 90 K as observed in the INS data.

IV. CONCLUSION

To summarize, we present a correlation between changes in the local structure and the magnetic susceptibility of FeAs. According to PDF analysis of short-range correlations, lattice parameters and bond distances increase overall with temperature, but in a complex and nonlinear way. In particular, the axial Fe-As bond distances increase with temperature revealing an overall $FeAs_6$ octahedral volume increase. Further, the $FeAs_6$ octahedral volume increases sharply between 200 and 300 K, which can be directly related to the magnetic susceptibility $\chi(T)$ result, which shows an anomalous broad feature up to 550 K, with χ continuing to increase above the Néel antiferromagnetic ordering temperature ($T_N = 70$ K), peaking at ~250 K, then decreasing gently above. Additionally, we carried out a detailed INS mapping of $S(Q; \hbar\omega)$ of magnetic excitations throughout reciprocal space at temperatures above and below the antiferromagnetic transition T_N. At low temperatures we observe gapped steeply dispersing anisotropic 3D spin waves extending to ~35 meV at zone boundaries. This is similar to the anisotropic 3D spin excitations observed in the superconducting iron-arsenide compounds, albeit those occur at much higher energy scale. Above T_N, the spin excitations become quasi-2D in both FeAs and superconducting iron-arsenide parent compounds like $BaFe_2As_2$. One thus expects a dimensional crossover from 2D magnetic fluctuations at elevated temperatures to 3D spin waves at ground state. The consequence of doping such a compound, and its potential to achieve unconventional superconductivity, is yet to be tested.

ACKNOWLEDGMENTS

This work was supported by the U.S. Department of Energy (DOE), office of Science, Basic Energy Sciences (BES), Materials Science and Engineering Division (MSE). This research used resources at the High Flux Isotope Reactor and Spallation Neutron Source, DOE office of Science User Facilities operated by the Oak Ridge National Laboratory. This manuscript has been authored by UT-Battelle, LLC, under Contract No. DE-AC05-00OR22725 with the U.S. Department of Energy (DOE). The U.S. government retains and the publisher, by accepting the article for publication, acknowledges that the U.S. government retains a nonexclusive, paid-up, irrevocable, worldwide license to publish or reproduce the published form of this manuscript, or allow others to do so, for U.S. government purposes. DOE will provide public access to these results of federally sponsored research in accordance with the DOE Public Access Plan [37].

[1] E. E. Rodriguez, C. Stock, K. L. Krycka, C. F. Majkrzak, P. Zajdel, K. Kirshenbaum, N. P. Butch, S. R. Saha, J. Paglione, and M. A. Green, Phys. Rev. B **83**, 134438 (2011).

[2] K. Segawa and Y. Ando, J. Phys. Soc. Jpn. **78**, 104720 (2009).

[3] Y. Kamihara, T. Watanabe, M. Hirano, and H. Hosono, J. Am. Chem. Soc. **130**, 3296 (2008).

[4] F.-C. Hsu, J.-Y. Luo, K.-W. Yeh, T.-K Chen, T.-W. Huang, P. M. Wu, Y.-C. Lee, Y.-L. Huang, Y-Y. Chu, D.-C. Yan, and M.-K. Wu, Proc. Natl. Acad. Sci. USA **105**, 14262 (2008).

[5] M. D. Lumsden and A. D. Christianson, J. Phys.: Condens. Matter **22**, 203203 (2010).

[6] J. Paglione and R. L. Greene, Nat. Phys. **6**, 645 (2010).

[7] P. S. Lyman and C. T. Prewitt, Acta Crystallogr. B **40**, 14 (1984).

[8] D. Gonzalez-Alvarez, F. Gronvold, B. Falk, E. F. Westrum Jr., R. Blachnik, and G. Kudermann, J. Chem. Thermodyn. **21**, 363 (1989).

[9] A. K. Jasek, K. Komdera, A. Bachowski, K. Ruebenbauer, J. Ukrowski, Z. Bukowski, and J. Karpinski, Philos. Mag. **95**, 493 (2015).

[10] S. Khim, M. Gillig, R. Klingeler, S. Wurmehl, B. Buchner, and C. Hess, Phys. Rev. B **93**, 205129 (2016).

[11] D. Parker and I. I. Mazin, Phys. Rev. B **83**, 180403(R) (2011).

[12] S. M. Griffin and N. A. Spaldin, J. Phys.: Condens. Matter **29**, 215604 (2017).

[13] S. O. Diallo, V. P. Antropov, T. G. Perring, C. Broholm, J. J. Pulikkotil, N. Ni, S. L. Bud'ko, P. C. Canfield, A. Kreyssig, A. I. Goldman, and R. J. McQueeney, Phys. Rev. Lett. **102**, 187206 (2009).

[14] L. W. Harriger, H. Q. Luo, M. S. Liu, C. Frost, J. P. Hu, M. R. Norman, and P. Dai, Phys. Rev. B **84**, 054544 (2011).

[15] R. A. Ewings, T. G. Perring, J. Gillett, S. D. Das, S. E. Sebastian, A. E. Taylor, T. Guidi, and A. T. Boothroyd, Phys. Rev. B **83**, 214519 (2011).

[16] J. T. Park, G. Friemel, T. Loew, V. Hinkov, Y. Li, B. H. Min, D. L. Sun, A. Ivanov, A. Piovano, C. T. Lin, B. Keimer, Y. S. Kwon, and D. S. Inosov, Phys. Rev. B **86**, 024437 (2012).

[17] J. Zhao, D. T. Adroja, D.-X. Yao, R. Bewley, S. Li, X. F. Wang, G. Wu, X. H. Chen, J. Hu, and P. C. Dai, Nat. Phys. **5**, 555 (2009).

[18] C. Zhang, L. W. Harriger, Z. Yin, W. Lv, M. Wang, G. Tan, Yu Song, D. L. Abernathy, W. Tian, T. Egami, K. Haule, G. Kotliar, and P. Dai, Phys. Rev. Lett. **112**, 217202 (2014).

[19] M. D. Lumsden, A. D. Christianson, E. A. Goremychkin, S. E. Nagler, H. A. Mook, M. B. Stone, D. L. Abernathy, T. Guidi, G. J. MacDougall, C. de la Cruz, A. S. Sefat, M. A. McGuire, B. C. Sales, and D. Mandrus Nat. Phys. **6**, 182 (2010).

[20] N. Murai, K. Suzuki, S.-i. Ideta, M. Nakajima, K. Tanaka, H. Ikeda, and R. Kajimoto Phys. Rev. B **97**, 241112(R) (2018).

[21] W. Lv, F. Kruger, and P. Phillips, Phys. Rev. B **82**, 045125 (2010).

[22] J. L. Niedziela, M. A. McGuire, and T. Egami, Phys. Rev. B **86**, 174113 (2012).

[23] B. A. Frandsen, K. M. Taddei, D. E. Bugaris, R. Stadel, M. Yi, A. Acharya, R. Osborn, S. Rosenkranz, O. Chmaissem, and R. J. Birgeneau, Phys. Rev. B **98**, 180505(R) (2018).

[24] B. Saparov, J. E. Mitchell, and A. S. Sefat, Supercond. Sci. Technol. **25**, 084016 (2012).

[25] J. Neuefeind, M. F. Feygenson, J. Carruth, R. Homann, and K. K. Chipley, Nucl. Instrum. Methods Phys. Res. B **287**, 68 (2012).

[26] C. L. Farrow, P. Juhas, J. W. Liu, D. Bryndin, E. S. Bozin, J. Bloch, T. Proffen, and S. J. L. Billinge, Condens. Matter **19**, 335219 (2007).

[27] G. Ehlers, A. Podlesnyak, J. L. Niedziela, E. B. Iverson, and P. E. Sokol, Rev. Sci. Instrum. **82**, 085108 (2011).

[28] G. Ehlers, A. Podlesnyak, and A. I. Kolesnikov, Rev. Sci. Instrum. **87**, 093902 (2016).

[29] G. E. Granroth, A. I. Kolesnikov, T. E. Sherline, J. P. Clancy, K. A. Ross, J. P. C. Ru, B. D. Gaulin, and S. E. Nagler, J. Phys. Conf. Ser. **251**, 012058 (2010).

[30] O. Arnold, J. C. Bilheux, J. M. Borreguero, A. Buts, S. I. Campbell, L. Chapon, M. Doucet, N. Draper, R. Ferraz Leal, M. A. Gigg, V. E. Lynch, A. Markvardsen, D. J. Mikkelson, R. L. Mikkelson, R. Miller, K. Palmen, P. Parker, G. Passos, T. G. Perring *et al.*, Nucl. Instrum. Methods. Phys. Res. A **764**, 156 (2014).

[31] R. Azuah, L. Kneller, Y. Qiu, P. Tregenna-Piggott, C. Brown, J. Copley, and R. Dimeo, J. Res. Natl. Inst. Stan. Technol. **114**, 341 (2009).

[32] G. Pokharel, A. F. May, D. S. Parker, S. Calder, G. Ehlers, A. Huq, S. A. J. Kimber, H. Suriya Arachchige, L. Poudel, M. A. McGuire, D. Mandrus, and A. D. Christianson, Phys. Rev. B **97**, 134117 (2018).

[33] P. Blaha, K. Schwarz, G. K. H. Madsen, D. Kvasnicka, J. Luitz, R. Laskowski, F. Tran, and L. D. Marks, *WIEN2k, An Augmented Plane Wave + Local Orbitals Program for Calculating Crystal Properties* (Karlheinz Schwarz, Techn. Universität Wien, Austria, 2018).

[34] J. P. Perdew, K. Burke, and M. Ernzerhof. Phys. Rev. Lett. **77**, 3865 (1996).

[35] K. Selte, A. Kjekshus, and A. F. Andresen. Acta Chem. Scand. **26**, 3101 (1972).

[36] P. C. Dai, J. Hu, and E. Dagotto, Nat. Phys. **8**, 709 (2012).

[37] http://energy.gov/downloads/doe-public-access-plan.